Journal of Energy Chemistry 52 (2021) 67–74

Contents lists available at ScienceDirect

Journal of Energy Chemistry

journal homepage: www.elsevier.com/locate/jechem

Block copolymer electrolyte with adjustable functional units for solid polymer lithium metal battery

Zhiyuan Lin [a,1], Xianwei Guo [a,1], Yubo Yang [a], Mingxue Tang [b], Qi Wei [a], Haijun Yu [a,*]

[a] College of Materials Sciences and Engineering, Key Laboratory of Advanced Functional Materials, Education Ministry of China, Beijing University of Technology, Beijing 100124, China
[b] Center for High Pressure Science & Technology Advanced Research, Beijing 100094, China

ARTICLE INFO

Article history:
Received 5 March 2020
Revised 23 April 2020
Accepted 23 April 2020
Available online 05 May 2020

Keywords:
Block copolymer electrolyte
Functional units
Ionic migration performance
Interface compatibility
Lithium metal battery

ABSTRACT

Solid polymer electrolytes have been considered as the promising candidates to improve the safety and stability of high-energy lithium metal batteries. However, the practical applications of solid polymer electrolytes are still limited by the low ionic conductivity, poor interfacial contact with electrodes, narrow electrochemical window and weak mechanical strength. Here, a series of novel block copolymer electrolytes with three-dimensional networks are designed by cross-linked copolymerization of the polyethylene glycol soft segments and hexamethylene diisocyanate trimer hard segments. Their ionic migration performances and interface compatibilities with Li metal anode have been optimized delicately by tailoring the ratio of these functional units. The optimized block copolymer electrolyte has shown an amorphous crystalline structure, a high ionic conductivity of ~5.7×10^{-4} S cm^{-1}, high lithium ion transference number (~0.49), wide electrochemical window up to ~4.65 V (vs. Li$^+$/Li) and favorable mechanical strength at 55 °C. Furthermore, the enhanced interface compatibility can well support the normal operations of lithium metal batteries using both $LiFePO_4$ and $LiNi_{0.8}Co_{0.15}Al_{0.05}O_2$ cathodes. This study not only paves a new way to develop solid polymer electrolyte with optimizing functional units, but also provides a polymer electrolyte design strategy for the application demand of lithium metal battery.

1. Introduction

The rechargeable lithium metal batteries (LMBs) are one of the hot spots of the current research in the electrochemical energy storage because of their high theoretical specific capacity (3860 mAh g^{-1}) and lowest redox potential (−3.04 V) [1–11]. However, the unavoidable growth of lithium (Li) dendrite during the repeated stripping/plating in liquid organic electrolytes could penetrate the separator, which causes the safety issue and prevents the practical applications of LMBs [12–17]. As one of the promising solve approaches, solid polymer electrolyte (SPE) has been applied to improve the safety and stability of LMBs [18–24]. However, the comprehensive properties of SPE, including the ionic conductivity, interfacial compatibility with electrode materials, electrochemical window and mechanical strength have enormous influences on the further applications [25–29]. For instance, although the poly(ethylene oxide) (PEO) has been explored widely in LMBs, it is still suffered by the low ionic conductivity, narrow electrochemical window and poor mechanical strength [30-36]. In order to overcome the above challenges, plenty of modifications have been explored, including the blend polymer electrolytes [37,38] and organic–inorganic composite electrolytes [28,39–42], to reduce the crystallinity of PEO structure, and improve the ionic conductivity, electrochemical window, and mechanical strength. However, the homogeneity of mixing two different materials is not easy to control. The properties of PEO-SPE still cannot meet the requirements of LMBs. Different from the blend/composite SPE, the block copolymer electrolyte (BCPE) has been proposed as homogeneous conductor from different polymer chains for the Li$^+$ migration. However, the comprehensive properties of BCPE are still not satisfactory for LMBs. Even more, there is few systematic study about the effect of different molecular chains on physical/chemical properties of BCPE.

In this work, we have designed a series of BCPE by the cross-linked copolymerization reaction via tailoring the ratio of functional units of polyethylene glycol (PEG) soft segment and Hexamethylene diisocyanate trimer (HDIt) hard segment, which are named PH-BCPE. As the different functional unit, the PEG soft segment has plenty of ether bonds in the backbone chains for Li$^+$ migrations (similar to the molecular structure of PEO) [43,44],

* Corresponding author.
E-mail address: hj-yu@bjut.edu.cn (H. Yu).
[1] These authors contributed equally to this work.

https://doi.org/10.1016/j.jechem.2020.04.052

while the glassy HDIt with hexamethylene unit possesses a good mechanical strength [45,46]. More importantly, the comprehensive properties of amorphous PH-BCPE with three-dimensional (3D) network structure can be optimized by tailoring the ratio of these functional units. It has been verified that the ionic conductivity of PH-BCPE and interfacial compatibility with Li metal anode can be enhanced by increasing the proportion of PEG functional unit, while the electrochemical window and mechanical property can be enlarged and improved respectively by increasing the proportion of HDIt functional unit. Furthermore, by optimizing the ratio of functional units, the PH-BCPE shows a high ionic conductivity of ~5.7×10^{-4} S cm^{-1}, high lithium ion transference number (~0.49), stable electrochemical window up to ~4.65 V (vs. Li^+/Li), and good interfacial compatibility with electrode at 55 °C. Accordingly, with the enhanced interface contact, the $LiFePO_4$/PH-BCPE/Li battery delivers a high discharge capacity of ~162 mAh g^{-1} at 0.1C (1C = 170 mA g^{-1}). Even with the $LiNi_{0.8}Co_{0.15}Al_{0.05}O_2$ cathode, the LMBs can offer the high discharge capacity of ~205 mAh g^{-1} at 0.1C when the charge potential is up to 4.6 V (vs. Li^+/Li). Therefore, the PH-BCPE reported in this study has proved the design strategy of SPE with comprehensive properties optimization, which can be achieved by tailoring the ratio of different functional units, and to be a promising candidate for the practical application in solid polymer LMBs.

2. Experimental

2.1. Fabrication of block copolymer electrolyte

The polyethylene glycol (PEG, M_w = 800 g mol^{-1}, 1500 g mol^{-1}, 10,000 g mol^{-1}), hexamethylene diisocyanate trimer (HDIt), aetonitrile (AN) and dibutyltin dilautrate (DBTDL) were purchased from Aldrich. The lithium bis(trifluoromethane sulfonyl imide) (LiTFSI) were supplied from Macklin. The PH-BCPE was fabricated by a solution-casting method. Firstly, HDIt (2.5 g), LiTFSI (5 g) and AN (20 mL) were added into the glass bottle under stirring to form a homogeneous solution in glove box. Then, PEG with different ratio with HDIt was added into the glass bottle to form a homogeneous solution under stirring. Subsequently, the DBTDL (2 wt%) as the catalyst was added into the solution and stirred for 3 h. Finally, the homogeneous solution was poured into the Whatman® filter (100% borosilicate glass fiber) on the Polytetrafluoroethylene (PTFE) plate followed by the polymerization in a vacuum at 60 °C for 12 h and then 80 °C for 6 h.

2.2. Characterization

The Fourier transform infrared spectroscopy (FT-IR) was carried out using a Nexus 870 FTIR spectrometer with the ATR instrument to distinguish the structures of PEG, HDIt, and PH-BCPE. The mechanical property of sample was investigated by an UTM4304 universal testing machine at a stretching speed of 1 mm min^{-1} and the hardness was checked by a shore durometer at 25 °C. The morphology and thickness of the samples were characterized by a field emission scanning electron microscope (SEM, Hitachi S-4800). The crystal structure of the PH-BCPE was characterized via XRD (Bruker D8 Advance) with range of 10°-80°. The high-resolution solid-state Magic Angle Spinning Nuclear Magnetic Resonance (MAS-NMR) spectra were obtained from on a Bruker 400 MHz spectrometer equipped with a Bruker 4.0 mm double resonance MAS probe at the ^{1}H and ^{13}C Larmor frequencies of 400.17 and 100.62 MHz, respectively. All samples were packed into 4.0 mm zirconia rotors with Kel-F drive caps in an Argon-filled glovebox, and were then spun at 6.0 kHz ± 3 Hz using a Bruker pneumatic MAS unit. The 90° pulse for ^{1}H excitation was determined as 2.9 μs and total 4 scans were accumulated for one spectrum. Longitudinal relaxation (T_1) measurements were performed using inversion recovery pulse sequence. For ^{13}C NMR measurements, all signals were recorded under the irradiation of single pulse length of 3.6 μs. High power decoupling was applied on ^{1}H during ^{13}C acquisition. For signal-averaging, total 512 transitions were accumulated for all samples. The ^{1}H and ^{13}C chemical shifts were referenced to the proton and the secondary carbon atom in adamantane at 1.8 and 38 ppm, respectively.

2.3. Electrochemical evaluation

The ionic conductivity of the PH-BCPE was tested by EIS using Versa STAT 3 system at various temperatures ranging from 25 °C to 85 °C. The PH-BCPE membranes were sandwiched between two stainless-steel (SS) plate electrodes and the spectra were recorded in the frequency range of 10^6 to 0.1 Hz with an AC amplitude of 10 mV. The bulk resistance (R_b) of PH-BCPE was determined from the impedance spectrum. The ionic conductivity was calculated from equation: $\sigma = L/R_bS$, where L and S are the thickness and area of the PH-BCPE, respectively. The electrochemical window was investigated by linear sweep voltammetry (LSV) performed from SS/PH-BCPE/Li battery at scan rate of 1.0 mV s^{-1} between 3 and 5.5 V (vs. Li^+/Li). The interface stability between Li anode and PH-BCPE was investigated by Cyclic Voltammograms (CV) that performed on SS/PH-BCPE/Li battery at scan rate of 1 mV s^{-1} from −1 to 2 V (vs. Li^+/Li). The lithium-ion transference number (t^+_{Li}) was calculated by the Chronoamperometry test on the Li/PH-BCPE/Li battery with an applied voltage of 0.01 V, and was determined by equation: $t^+_{Li} = \frac{I_{ss}}{I_0} \times \frac{V-I_0R_0}{V-I_{ss}R_{ss}}$, where I_0 and I_{ss} are the initial and steady-state currents, and R_0 and R_{ss} are the first and last resistances, respectively. The tests were completed by EIS measurements that taken before and after the polarization scans over a frequency range of 10^6 to 0.1 Hz with a 10 mV amplitude at 55 °C.

2.4. Battery test

The $LiFePO_4$ or $LiNi_{0.8}Co_{0.15}Al_{0.05}O_2$ (NCA) cathode was prepared by pasting the mixture of 80 wt% $LiFePO_4$ /NCA, 10 wt% carbon black, and 10 wt% binder (PVDF:PH-BCPE = 7:3) on the Al current collector. The loading mass of active materials was controlled with areal density of 2.0–3.0 mg cm^{-2}. The CV test of $LiFePO_4$/PH-BCPE/Li battery was conducted at scan rate of 0.1 mV s^{-1} between 2 and 4.25 V (vs. Li^+/Li). The $LiFePO_4$/PH-BCPE/Li battery was charged and discharged between 2.5 and 4.0 V at different current densities. The C rates are defined based on 1C = 170 mA g^{-1}. The NCA/PH-BCPE/Li battery was charged and discharged between 2.8 and 4.3 V or 4.6 V at 0.1C (1C = 200 mA g^{-1}). The galvanostatic charge/discharge tests of coin-type batteries (CR2032) were conducted on LAND testing system (Wuhan LAND Electronics Co., Ltd.) at 55 °C.

3. Results and discussion

A series of PH-BCPE have been fabricated by cross-linked copolymerization reaction from different ratio of functional units of PEG soft and HDIt hard segments, in which the proportion can be tailored with n_{PEG}/n_{HDIt} as R value. Fig. 1(a) shows the typical copolymerization process from the PEG and HDIt precursors, and the corresponding cross-linked 3D network structure of PH-BCPE. For the detail, the PEG has the polyether backbone with hydroxies on both terminals, while the HDIt has the hexamethylene units with isocyanate on three terminals. For the R = 1.5, the PH-BCPE with cross-linked 3D network structure can be obtained after the

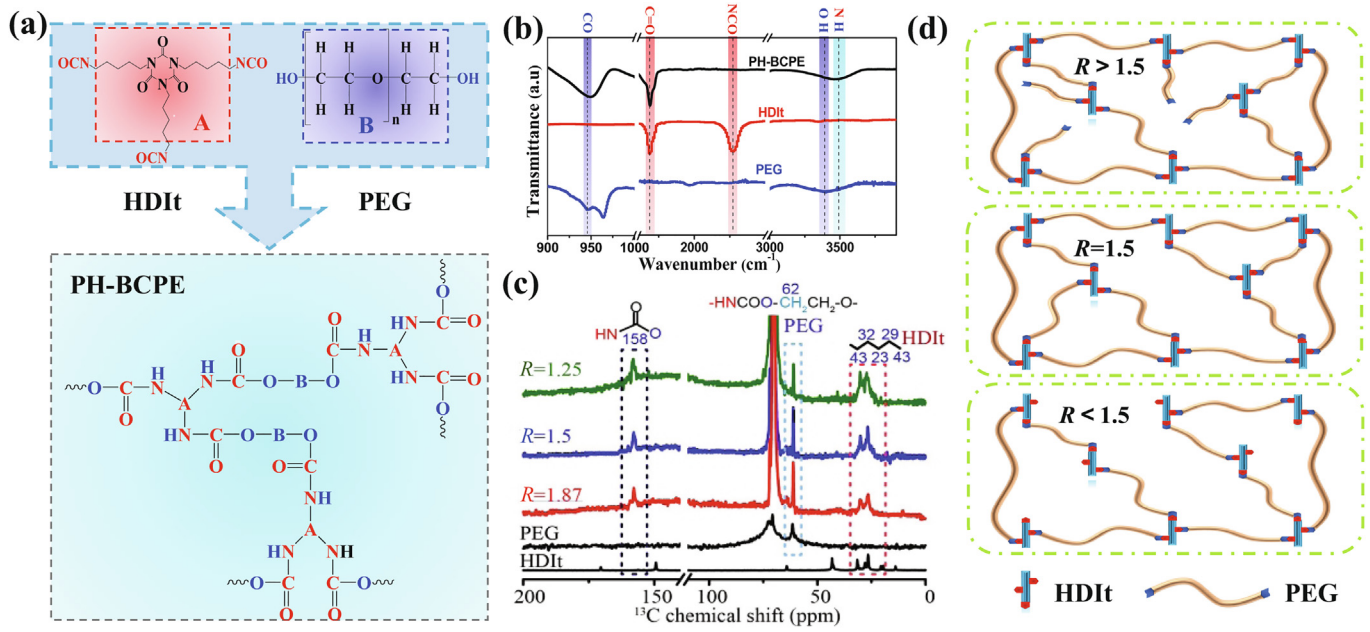

Fig. 1. (a) The molecular structures of PEG and HDIt functional units, and the PH-BCPE with cross-linked 3D network structure by the copolymerization with R = 1.5. (b) The FT-IR spectra of PEG, HDIt and PH-BCPE with R = 1.5. (c) The ^{13}C MAS NMR spectra of PEG, HDIt and PH-BCPE with different R value. (d) The schematic diagram of PH-BCPE with different ratios of functional units.

full copolymerization of hydroxy (–OH) from PEG soft segment and isocyanate (–N–C═O) from HDIt hard segment, in which the new [–N–(C═O)–O–] bond as the cross-linking part (the lower part in Fig. 1a), without any change of the backbone chain.

The copolymerization mechanism of PH-BCPE from different functional units of PEG soft and HDIt hard segment has been verified by Fourier Transform Infrared Spectroscopy (FT-IR). When the value of R is 1.5, both of the typical absorption peak of –OH bond in PEG at ~3400 cm^{-1} and –N–C═O bond in HDIt at ~2276 cm^{-1} disappeared, following by the formation of new peak of –NH bond at ~3500 cm^{-1} (Fig. 1b). It has indicated the polymerization of PH-BCPE between –OH from PEG soft segment and –N–C═O from HDIt hard segment. Meanwhile, there was no obvious shift of peak position of C-O bond (~945 cm^{-1}) and C═O bond (~1700 cm^{-1}), indicating the stability of –C–O in PEG and –C═O in HDIt before and after the copolymerization process, which is beneficial for the Li$^+$ migration inside PH-BCPE. From the scanning electron microscopy (SEM) image of PH-BCPE with R = 1.5 (Fig. S1a), it is clear that the surface of PH-BCPE is smooth with homogeneity, which is favorable for the strong adhesion to the electrode with good interface compatibility. From the cross-sectional SEM image of PH-BCPE, the homogeneous structure with the thickness of ~150 μm has been achieved, which can effectively prevent the possible inner short-circuit and improve the safety and stability of LMBs (Fig. S1b). Furthermore, the PH-BCPE has good flexibility with favorable mechanical property (insert in Fig. S1c), which are suitable for making the flexible batteries or electronic device with variable shape.

In order to detect the local structure of PH-BCPE copolymer and understand the copolymerization process from PEG and HDIt functional units, the well-resolved solid state MAS-NMR spectra have been conducted and analyzed (Fig. 1c). Obviously, high-resolution peaks for the samples before and after the copolymerization are well assigned to the correlated carbons. At the bottom of Fig. 1(c), two resonances at 62 ppm and 70 ppm can be clearly seen for the sorts of carbons in PEG functional unit, and a series of peaks between 20 and 45 ppm are from the typical aliphatic carbons in HDIt functional unit. After copolymerization, a new peak at 158 ppm appears no matter the variation of R value, indicating the formation of –NH–CO–O– bond between –OH in PEG and –N═C═O in HDIt. Furthermore, with the R value increase, the intensities of characteristic peaks in PEG increases, while the intensities of characteristic peaks in HDIt decreases simultaneously. It has demonstrated that the microstructures of PH-BCPE can be designed and adjusted by tailoring the ratio between PEG and HDIt functional units to achieve optimized properties of PH-BCPE. Moreover, the ^{1}H NMR studies in Fig. S2 can also consolidate the results obtained from the ^{13}C NMR study. The ^{1}H longitudinal relaxation rates ($1/t_1$) increase significantly (~5 times) from pure PEG (t_1 = 3.33 s) to PH-BCPE (t_1 ~0.60 s), reflecting the enhanced mobility of protons attached to PH-BCPE chain, which is probably beneficial for improving the ionic conductivity [47-49]. The differences observed for ^{1}H relaxation times should be attributed to different R value for PH-BCPE. Therefore, the microstructure design of PH-BCPE can be improved by tuning of PEG soft segment and HDIt hard segments. Fig. 1(d) shows the schematic diagram of the corresponding microstructure of PH-BCPE with different ratio of functional units. It has been pointed out that the PEG with polyether backbone is beneficial for Li$^+$ migration, while the HDIt with glassy state has a good mechanical strength. Furthermore, with high fraction of PEG functional unit, the interfacial contact with electrodes can also be improved. Therefore, it can be estimated that the Li$^+$ migration, interfacial compatibility, and mechanical strength of PH-BCPE can be optimized by tailoring the ratio of functional units of PEG soft and HDIt hard segments.

Accordingly, the fundamental properties of PH-BCPE with different ratio of functional units have been systematically explored. The ionic conductivity (σ) of SPE has a critical role for improving the performances of polymer LMBs. Thus, σ of PH-BCPE has been evaluated firstly with different ratio of functional unit by ranging R value from 1.25 to 2.14 at 25 °C (Fig. 2a), and the results have been obtained by the bulk resistance (R_b) of SPE film (insert in Fig. 2a) from the electrochemical impedance spectra (EIS) of SS/PH-BCPE/SS (SS: stainless steel) symmetrical battery. It can be found that the R_b decreases gradually with the increase of R value, indicating that the σ of PH-BCPE increase simultaneously (Fig. 2a). More importantly, the σ of PH-BCPE can be increased from

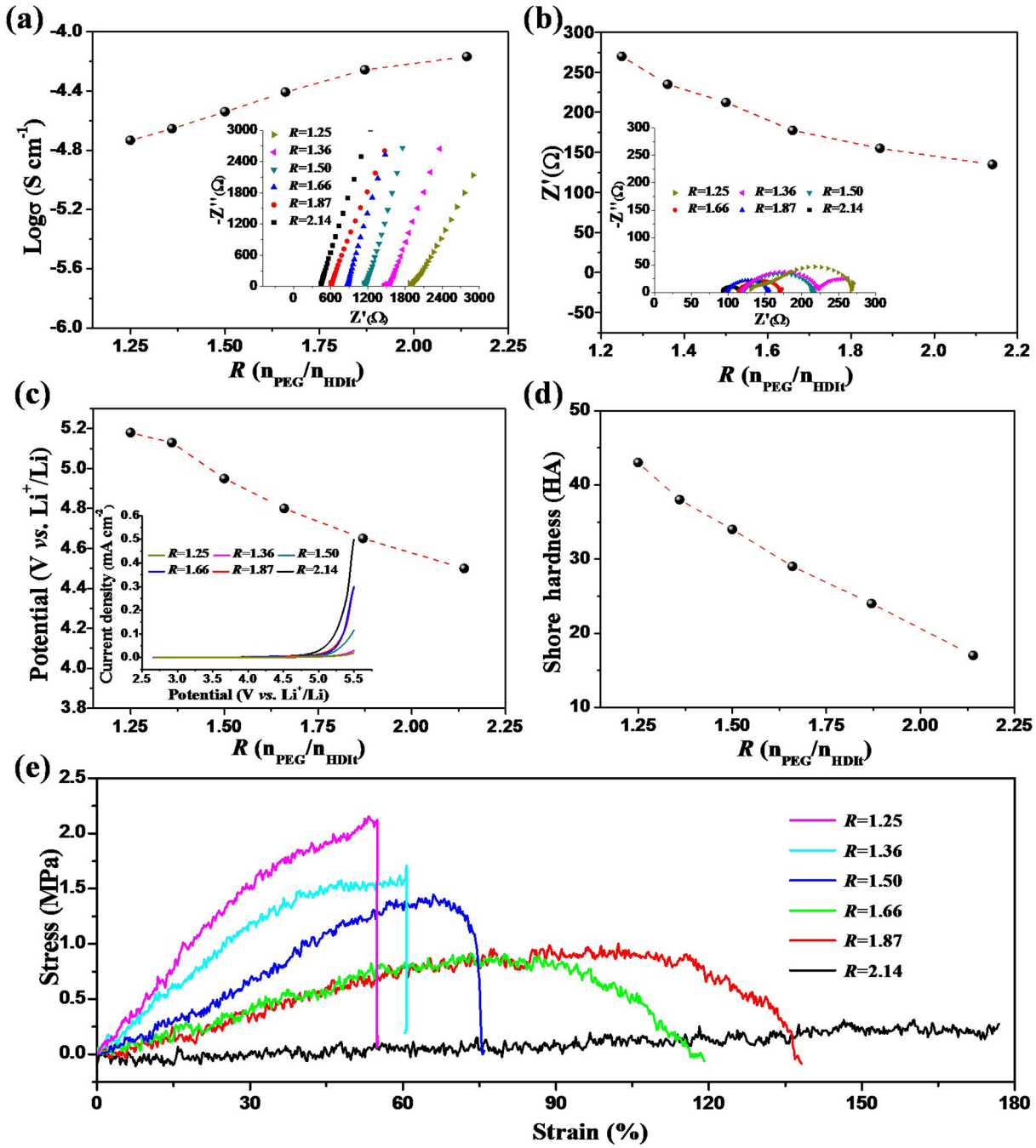

Fig. 2. (a) The relationship between ionic conductivity of PH-BCPE and functional unit with different *R* values. The insert is the EIS of SS/PH-BCPE/SS symmetric battery with different *R* values. (b) The EIS (insert) and interfacial resistance of Li/PH-BCPE/Li symmetric battery with different *R* values. (c) The electrochemical window of PH-BCPE with different *R* values. (d) Shore hardness and (e) stress–strain curves of PH-BCPE with different *R* values.

2.1×10^{-5} S cm^{-1} with R = 1.25 to 7.8×10^{-5} S cm^{-1} with R = 2.14 at 25 °C. It has demonstrated that the σ of PH-BCPE can be enhanced by increasing the ratio of PEG functional unit. The interactions between Li^+ and ether bonds comprising oxygen in the backbone chains of PEG soft segment are favor for the fast ions migrations. In addition, the –C–N and –C═O bonds in hexagonal ring structure of HDIt hard segment and the cross-linking part of [–N–(C═O)–O–] bond may also be useful for the Li^+ migrations [50,51].

The structure of PH-BCPE with different ratio of functional unit has been detected by X-ray diffraction (XRD). As seen in Fig. S3, different from the high crystallinity of PEO [52], there is only a broad peak of PH-BCPE, indicating the amorphous structure, which is beneficial for the Li^+ migration [53]. Furthermore, the interfacial compatibility between PH-BCPE and electrodes could also be enhanced by the amorphous structure, which is important for the practical applications of LMBs. Besides the structure of functional unit, the effect of length of PEG segment with different molecular weight on the framework and ionic conductivity of PH-BCPE has been explored (Fig. S4), indicating that the length of molecular chain in PEG can also influence the ions migration ability. Furthermore, the interfacial resistance (R_i) of Li/PH-BCPE/Li symmetrical battery with different *R* value has been compared. From the EIS of Li/PH-BCPE/Li symmetrical batteries with different

R values at 55 °C (inset in Fig. 2b), there is an obvious decrease of R_i with the increase of *R* value in Fig. 2(b), similar to the tendency in SS/PH-BCPE/SS battery (insert in Fig. 2a). It can be found that the R_i of Li/PH-BCPE/Li battery for *R* = 1.25 (~270 Ω) is much higher than that of R_i for *R* = 2.14 (~135 Ω). Thus, similar to the increase of ionic conductivity, the significant reduction of interfacial resistance between PH-BCPE and Li metal anode can be achieved via increasing the fraction of PEG functional unit, which can further improve the electrochemical performances of polymer LMBs.

The electrochemical window of SPE is also one of the crucial parameters for practical application in LMBs. By a linear sweep voltammetry (LSV) of an asymmetrical battery of Li/PH-BCPE/SS at 55 °C (Fig. 2c), it can be seen that the PH-BCPE is stable up to ~5.15 V (vs. Li^+/Li) for *R* = 1.25, which is favorable for the promising application for high-potential cathode material in solid polymer LMBs. However, the electrochemical window of PH-BCPE decreases greatly with the increase of *R* value, and still be close to ~4.5 V (vs. Li^+/Li) for *R* = 2.14. Therefore, it has revealed that the electrochemical window of PH-BCPE can be enlarged by increasing the fraction of HDIt functional unit.

It has been proved that the mechanical strength plays an important role in the application of polymer electrolyte, especially for the suppression of Li dendrite in polymer LMBs. The mechanical property of PH-BCPE with different ratio of functional units was investigated by tensile and hardness testing. Fig. 2(d) exhibits the relationship between Shore hardness of PH-BCPE and functional units with various *R* value ranging from 1.25 to 2.14. Obviously, the hardness of PH-BCPE is ~42 HA for *R* = 1.25, which is much higher than that of ~17 HA for *R* = 2.14. More importantly, there is an approximately linear relationship between hardness and *R* value at the testing range, indicating the enhancement of Shore hardness of PH-BCPE with the increase of HDIt functional unit. Furthermore, from the stress–strain curves of the PH-BCPE with different *R* value in Fig. 2(e), it can be found that the stress is ~2.1 MPa for *R* = 1.25. However, when the *R* increases to 2.12, the stress of PH-BCPE is only ~0.2 MPa, which was not favorable for the safety and reliability of solid polymer LMBs. Similar to that of Shore hardness, the stress of PH-BCPE has increased greatly by increasing the proportion of HDIt functional unit. Thus, besides the electrochemical window adjustment, the mechanical property of PH-BCPE can also be tailored by increasing the fraction of HDIt functional unit, which can further improve the safety and reliability of polymer LMBs by alleviating the possible short circuit inside the batteries.

As discussed above, if *R* value is equal to 1.5, the –OH from PEG soft segment and –N–C═O from HDIt hard segment can be fully copolymerized for the PH-BCPE formation. More importantly, it has been sufficiently confirmed that the comprehensive properties of PH-BCPE could be optimized by tailoring the ratio of functional units of PEG soft and HDIt hard segments. For instance, the ionic conductivity and interfacial contact can be enhanced by increasing the proportion of PEG soft segment (*R* > 1.5) in PH-BCPE, which may be beneficial for improving the rate performance and reducing the interfacial resistance of solid polymer LMBs. In contrast, with the increase of proportion of HDIt hard segment (*R* < 1.5), the electrochemical window and mechanical property of PH-BCPE can be enlarged and improved respectively, which can be available for high-potential cathode material in solid polymer LMBs with improved safety and reliability. Therefore, the design of PH-BCPE can be achieved by tailoring the ratio of functional units of PEG soft and HDIt hard segments.

For the application of SPE in polymer LMBs, the optimized features with high ionic conductivity and small interface resistance need to be mainly considered, and the relative high electrochemical window and mechanical strength should also be suitable for the assembling of solid battery. Thus, the optimized PH-BCPE with high proportion of PEG soft segment (*R* = 1.87) has been systematically explored in the following polymer LMBs. Firstly, the temperature dependency of the ionic conductivity of PH-BCPE at temperature range of 25 to 85 °C has been evaluated in Fig. 3(a), in which the result has been calculated by the R_b that obtained from the EIS of SS/PH-BCPE/SS symmetrical battery at different temperature (Fig. S5). It can be found that the ionic conductivity of PH-BCPE increase simultaneously with the increase of temperature, that is, from 6.51×10^{-5} S cm^{-1} at 25 °C, to 5.7×10^{-4} S cm^{-1} at 55 °C, and then 1.12×10^{-3} S cm^{-1} at 85 °C. It has been illustrated that the fast ions migrations can be achieved by the interactions between Li^+ and different chemical bonds, including the ether bonds comprising oxygen in the backbone chains of PEG segment, the –C–N and –C═O bonds in hexagonal ring structure of HDIt segment, and the cross-linking part of [–N–(C═O)–O–] bond. Furthermore, the ionic conductivity of PH-BCPE depending on temperature can be fitted by the Arrhenius plot, and the low activation energy of 0.208 eV can be obtained, indicating the low energy barrier that is beneficial for Li^+ migration. Moreover, the linear relationship between $\log\sigma$ and $1000/T$ has revealed the structural stability of PH-BCPE within the temperature range, which has been further confirmed by the partially increase of R_b with the aging time of 21 days (Fig. S6).

The Li^+ transference number (t_{Li}^+) is also one of the important parameters for determining the side reaction on the surface of electrodes and the polarization of LMBs. As shown in Fig. 3(b), from the direct current polarization and EIS tests, it can be calculated that the t_{Li}^+ of PH-BCPE is ~0.49 at 55 °C, which is higher than that of the common liquid electrolyte. The high t_{Li}^+ of PH-BCPE should be attributed to the strong inhibiting effect of anoins ($TFSI^-$) movement by the 3D cross-linked network structure in PH-BCPE, which is favorable for increasing the Li^+ migration, reducing the concentration polarization and improving the rate performance of LMBs [45]. Furthermore, from the EIS of Li/PH-BCPE/Li symmetrical battery before and after polarization test (inset in Fig. 3b), there is no obvious change of R_b and R_i, indicating the stable bulk structure and interfacial contact with Li metal anode. Therefore, the PH-BCPE has an enhanced interface contact with small resistance toward Li metal anode, which is helpful for improving the electrochemical performances of polymer LMBs.

Besides the interfacial contact, the electrochemical stability between PH-BCPE and Li metal anode has also been explored by the Cyclic Voltammograms (CV) test of Li/PH-BCPE/SS battery in a voltage range of −1.0 to 2.0 V (vs. Li^+/Li) at 55 °C (Fig. S7). There is only a lithium plating peak at −0.86 V (*vs.* Li^+/Li) and reversible stripping peak at 0.45 V (vs. Li^+/Li) in a scan cycle, indicating the electrochemical interface stability of PH-BCPE toward Li metal anode. Furthermore, the stable interfacial contact between PH-BCPE and Li metal anode has been investigated by the polarization test of Li/PH-BCPE/Li symmetric battery at 0.1 mA cm^{-2} for 1 h at 55 °C (Fig. 3c). It can be found that the battery can work for 300 h without short circuiting, which shows high cycling reversibility and stability for lithium plating/stripping in PH-BCPE based LMBs. In detail, there is a slight increase of the plating voltage from ~50 mV at the initial cycle to ~60 mV after 300 h in the symmetric battery. The low voltage polarization of Li plating/stripping in Li/PH-BCPE/Li symmetric battery should be attributed to the excellent interfacial compatibility between amorphous PH-BCPE and Li metal anode. Even more, the morphologies of Li deposits in PH-BCPE and liquid electrolyte have been recorded by SEM after 300 cycles with the same current density (Fig. 3d–f). Compared to the smooth surface of pristine Li metal in Fig. 3(d), the porous Li dendrite on the surface of metal anode can be found for the liquid electrolyte based battery, and much easier to lose contact with electrons among deposits (Fig. 3e), which should be caused by the unstable interface contact between liquid electrolyte and Li

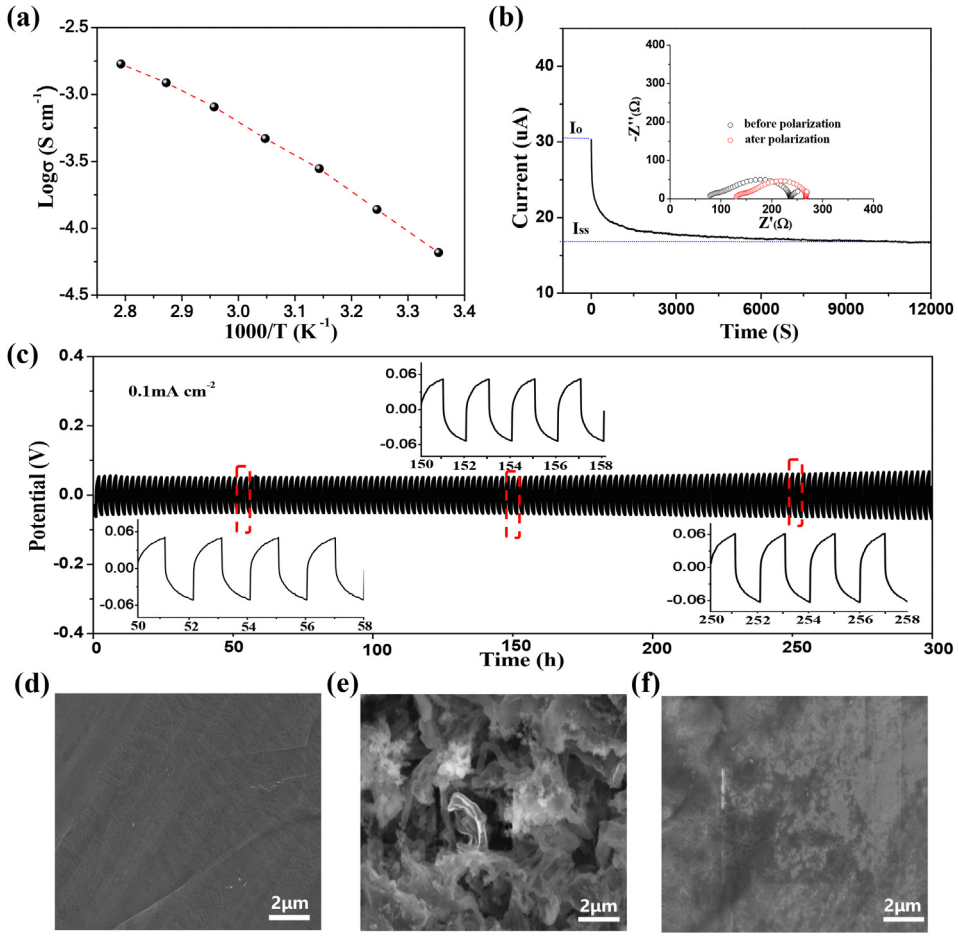

Fig. 3. (a) The temperature dependency of ionic conductivity of PH-BCPE with R = 1.87. (b) The chronoamperometry profile of symmetric Li/PH-BCPE/Li battery, and the EIS before and after the polarization (insert). (c) The potential profiles of repeated Li plating/striping using PH-BCPE at 0.1 mA cm^{-2} over 300 h. The SEM images of the surfaces of Li metal at different states: (d) pristine, (e) cycled in liquid electrolyte, and (f) cycled with PH-BCPE.

metal anode. On the contrast, there is no obvious Li dendrite on the surface of metal anode for the PH-BCPE based symmetric battery (Fig. 3f). The obvious suppression of Li dendrite should be attributed to the enhanced interface contact between PH-BCPE and Li metal anode, and the favorably mechanical strength that provided by the functional unit of HDIt hard segment. Therefore, the intimately interfacial compatibility with low interfacial resistance and high stability between PH-BCPE and Li metal anode are beneficial for enhancing the electrochemical performances of polymer LMBs.

The solid polymer LMBs based on PH-BCPE and $LiFePO_4$ (LFP) cathode have been assembled and the electrochemical performances have been explored. Fig. 4(a) shows the typical charge–discharge curves of LFP/PH-BCPE/Li battery between 2.5–4.0 V at the current density of 0.1C (1C = 170 mA g^{-1}) at 55 °C. It can be seen that the discharge capacity is ~162 mAh g^{-1} with the Coulombic efficiency of 98.6%, which should be attributed to the high ionic conductivity of PH-BCPE, and the excellent interface compatibility with electrodes. Besides, the battery exhibits the stable potential plateaus with low over-potential between charge/discharge curves, which has been further proved by the CV test (Inset in Fig. 4a). Moreover, the cycling stability of LFP/PH-BCPE/Li battery is obtained at 1C under the same condition (Fig. 4b). The reversible capacity is ~141 mAh g^{-1} for the initial cycle and decreases to ~120 mAh g^{-1} over 100 cycles, while the Coulombic efficiency is near 99%. The obvious variation of over-potentials between charge and discharge curves (insert in Fig. 4b) as well as the capacity fading after hundreds of cycles should be caused by the polarization effect of polymer LMBs at the high current density for long time, which has been confirmed by the EIS of LFP/PH-BCPE/Li battery at different cycles. From Fig. S8, the interfacial resistances of LFP/PH-BCPE/Li battery keep increasing with the increase of cycles, which should be caused by the aging of interface contact between PH-BCPE and electrodes that accelerated at high temperature during charging and discharging, consisting with the increase of over-potentials for long cycling.

Fig. 4(c) exhibits the rate performances of LFP/PH-BCPE/Li battery with the current densities increase from 0.1C to 2C at 55 °C. With the improved interface compatibility, the battery shows a high specific capacity of ~153 mAh g^{-1} at low current density of 0.5C, and ~133 mAh g^{-1} at current density of 1C. Even at a higher current density of 2C, the specific capacity is still keeps at ~78 mAh g^{-1}. The increase of over-potential and fading of capacity with the increase of current density should originated from the limited Li^+ migration rate in the solid electrolyte (inset in Fig. 4c). Furthermore, it has been pointed out that the PH-BCPE (R = 1.87) with the electrochemical window of ~4.65 V (vs. Li^+/Li) can be used for high-potential cathode material. Thus, the polymer LMBs based on $LiNi_{0.8}Co_{0.15}Al_{0.05}O_2$ (NCA) with higher charge potentials have been investigated. Obviously, the NCA/PH-BCPE/Li battery shows a high initial discharge capacity of ~188 mAh g^{-1} with the Coulombic efficiency of ~90.7% at the current density of 0.1C (1C = 200 m A g^{-1}) under the terminal charge potential of 4.3 V at 55 °C (Fig. 4d). Furthermore, the higher discharge capacity of ~205

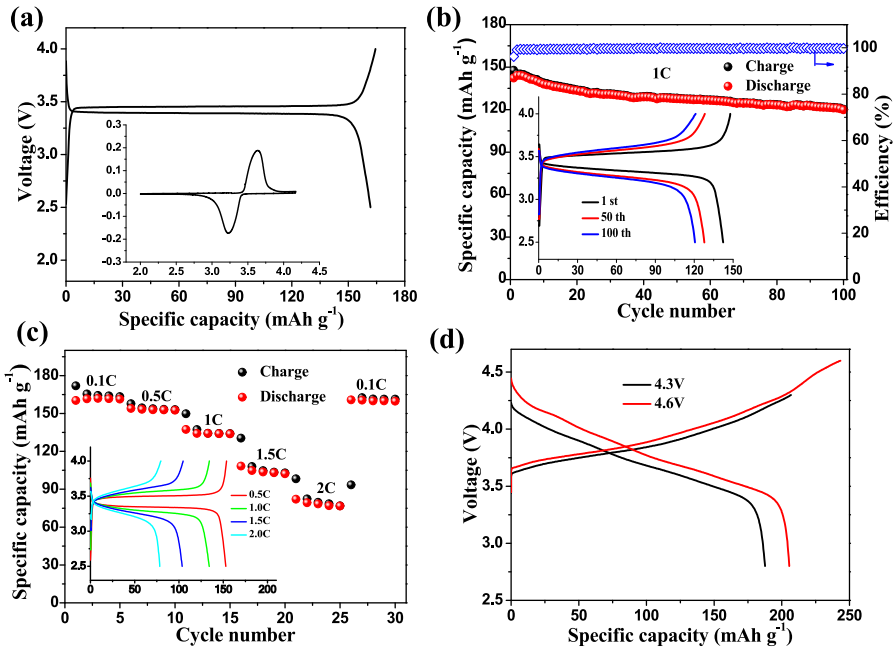

Fig. 4. (a) The initial charge and discharge curves of $LiFePO_4$ cathode with PH-BCPE at 0.1C. The inset is the corresponding CV curve for the battery. (b) Cycling performance of $LiFePO_4$/PH-BCPE/Li battery at 1C. The inset is the selected charge–discharge curves with different cycles. (c) Rate performances of $LiFePO_4$/PH-BCPE/Li battery. The inset is the selected charge–discharge curves with different rates. (d) The initial charge and discharge curves of $LiNi_{0.8}Co_{0.15}Al_{0.05}O_2$/PH-BCPE/Li battery at 0.1C with different charge potentials. All of the batteries are tested at 55 °C.

mAh g^{-1} can be obtained when the charge potential up to 4.6 V. Therefore, with the high ionic conductivity and good interface contact between SPE and electrodes that offered by the high proportion of functional unit of PEG soft segment, and the high electrochemical window and favorable mechanical strength by the functional unit of HDIt hard segment, the PH-BCPE can be applied in the high-energy polymer LMBs.

4. Conclusions

In summary, we have designed a series of block copolymer electrolytes (PH-BCPE) by the cross-linked copolymerization reaction from different functional units of PEG soft and HDIt hard segments. It has been verified that the comprehensive properties of the amorphous PH-BCPE with 3D network structure can be optimized delicately by tailoring the ratio of functional units, in which the ionic conductivity of PH-BCPE and interfacial compatibility with Li metal anode can be enhanced by increasing the proportion of PEG soft segment, while the electrochemical window and mechanical property can be enlarged and improved respectively by increasing the proportion of HDIt hard segment. By using the optimized PH-BCPE with enhanced interface contact, the solid polymer LMBs composed of $LiFePO_4$ cathode can deliver highly reversible capacity and good rate performances, even can be charged to 4.6 V with the $LiNi_{0.8}Co_{0.15}Al_{0.05}O_2$ cathode. Therefore, this study not only demonstrates a new way to develop solid polymer electrolyte with optimizing functional units, but also provides a polymer electrolyte design strategy for the application demand of LMBs.

Declaration of Competing Interest

The authors declare that they have no known competing financial interests or personal relationships that could have appeared to influence the work reported in this paper.

Acknowledgments

This work was supported financially by the National Key R&D Program of China (Grant No. 2018YFB0104300), Beijing Natural Science Foundation (JQ19003, KZ201910005002 and L182009), National Natural Science Foundation of China (Grants 21875007, 51622202, and 21974007), and the Project of Youth Talent Plan of Beijing Municipal Education Commission (CIT&TCD201804013).

Appendix A. Supplementary data

Supplementary data to this article can be found online at https://doi.org/10.1016/j.jechem.2020.04.052.

References

[1] H. Kin, G. Jeong, Y. Kim, J. Kim, C. Parke, H. Sohn, Chem. Soc. Rev. 42 (2013) 9011–9034.
[2] W. Xu, J. Wang, F. Ding, X. Chen, E. Nasybulin, Y. Zhang, J.G. Zhang, J.G. Zhang, Energy Environ. Sci. 7 (2014) 513–537.
[3] A. Manthiram, X. Yu, S. Wang, Nat. Mater. 2 (2017) 16103.
[4] X.B. Cheng, R. Zhang, C.Z. Zhao, Q. Zhang, Chem. Rev. 117 (2017) 10403–10473.
[5] D. Lin, Y. Liu, Y. Cui, Nat. Nanotech. 12 (2017) 194–206.
[6] Y. Guo, H. Li, T. Zhai, Adv. Mater. 29 (2017) 1700007.
[7] Q. Liu, Z. Geng, C. Han, Y. Fu, S. Li, Y.B. He, F. Kang, B. Li, J. Power Sources 389 (2018) 120–134.
[8] L. Fan, S. Wei, S. Li, Q. Li, Y. Lu, Adv. Energy Mater. 8 (2018) 1702657.
[9] F. Wu, Y.X. Yuan, X.B. Cheng, Y. Bai, Y. Li, C. Wu, Q. Zhang, Energy Storage Mater. 15 (2018) 148–170.
[10] H. Yu, Y.G. So, Y. Ren, T. Wu, G. Guo, R. Xiao, J. Lu, H. Li, Y. Yang, H. Zhou, R. Wang, K. Amine, Y. Ikuhara, J. Am. Chem. Soc. 140 (2018) 15279–15289.
[11] X. Chen, W. He, L. Ding, S. Wang, H. Wang, H. Wang, Energy Environ. Sci. 12 (2019) 938–944.
[12] Y. Lu, Z. Tu, L.A. Archer, Nat. Mater. 13 (2014) 961–969.
[13] K.J. Harry, D.T. Hallinan, D.Y. Parkinson, A.A. MacDowell, N.P. Balsara, Nat. Mater. 13 (2014) 69–73.
[14] W. Li, H. Yao, K. Yan, G. Zheng, Z. Liang, Y.M. Chiang, Y. Cui, Nat. Commun. 6 (2015) 7436.
[15] K. Yan, Z. Lu, H.W. Lee, F. Xiong, P.C. Hsu, Y. Li, J. Zhao, S. Chu, Y. Cui, Nat. Energy 1 (2016) 16010.
[16] J. Zhang, J. Yang, T. Dong, M. Zhang, J. Chai, S. Dong, T. Wu, X. Zhou, G. Cui, Small 14 (2018) 1800821.

[17] H. Wu, Y. Cao, H. Su, C. Wang, Angew. Chem. Int. Ed. 57 (2018) 1361–1365.
[18] H. Duan, Y. Yin, X. Zeng, J. Li, J. Shi, Y. Shi, R. Wen, Y. Guo, L. Wan, Energy Storage Mater. 10 (2018) 85–91.
[19] J. Zhang, J. Zhao, L. Yue, Q. Wang, J. Chai, Z. Liu, X. Zhou, H. Li, Y. Guo, G. Cui, L. Chen, Adv. Energy Mater. 5 (2015) 1501082.
[20] Y. Kato, S. Hori, T. Saito, K. Suzuki, M. Hirayama, A. Mitsui, M. Yonemura, H. Iba, R. Kanno, Nat. Energy 1 (2016) 16030.
[21] Na. Wu, Y. Shi, S. Lang, J. Zhou, J. Liang, W. Wang, S. Tan, Y. Yin, R. Wen, Y. Guo, Angew. Chem. Int. Ed. 10 (2018) 18146–18149.
[22] W. Zhou, S. Wang, Y. Li, S. Xin, A. Manthiram, J.B. Goodenough, J. Am. Chem. Soc. 138 (2016) 9385–9388.
[23] X.X. Zeng, Y.X. Yin, N.W. Li, W.C. Du, Y.G. Guo, L.J. Wan, J. Am. Chem. Soc. 138 (2016) 15825–15828.
[24] H. Gao, L. Xue, S. Xin, J.B. Goodenough, Angew. Chem. Int. Ed. 57 (2018) 5449–5453.
[25] M. Mushtaq, X.W. Guo, J.P. Bi, Z.X. Wang, H.J. Yu, Rare Met. 37 (2018) 520–526.
[26] T. Dong, J. Zhang, G. Xu, J. Chai, H. Du, L. Wang, H. Wen, X. Zang, A. Du, Q. Jia, X. Zhou, G. Cui, Energy Environ. Sci. 11 (2018) 1197–1203.
[27] C. Ma, K. Dai, H. Hou, X. Ji, L. Chen, D.G. Ivey, W. Wei, Adv. Sci. 5 (2018) 1700996.
[28] J. Bae, Y. Li, J. Zhang, X. Zhou, F. Zhao, Y. Shi, J.B. Goodenough, G. Yu, Angew. Chem. Int. Ed. 57 (2018) 2096–2100.
[29] H. Zeng, X. Ji, F. Tsai, Q. Zhang, T. Jiang, R.K.Y. Li, H. Shi, S. Luan, D. Shi, Solid State Ionics 320 (2018) 92–99.
[30] M. Armand, Adv. Mater. 2 (1990) 278–286.
[31] Z. Zhang, D. Sherlock, R. West, R. West, Macromolecules 36 (2003) 9176–9180.
[32] N.P. Balsara, E.D. Gomez, A. Panday, E.H. Feng, V. Chen, G.M. Stone, A.M. Minor, C. Kisielowski, K.H. Downing, O. Borodin, G.D. Smith, Nano Lett. 9 (2009) 1212–1216.
[33] Z. He, L. Fan, Rare Met. 37 (2018) 488–496.
[34] K. Xu, Chem. Rev. 114 (2014) 11503–11618.
[35] Z. Hu, S. Zhang, S. Dong, W. Li, H. Li, G. Cui, L. Chen, Chem. Mater. 29 (2017) 4682–4689.
[36] A.B. Puthirath, S. Patra, S. Pal, M. Manoj, A.P. Balan, S. Jayalekshmi, N.N. Tharangattu, J. Mater. Chem. A 5 (2017) 11152–11162.
[37] C. Tao, M.H. Gao, B.H. Yin, B. Li, Y.P. Huang, G. Xu, J.J. Bao, Electrochim. Acta. 257 (2017) 31–39.
[38] D. Zhang, L. Zhang, K. Yang, H. Wang, C. Yu, D. Xu, B. Xu, L.M. Wang, ACS Appl. Mater. Interf. 9 (2017) 36886–36896.
[39] J. Zhang, N. Zhao, M. Zhang, Y. Li, P.K. Chu, X. Guo, Z. Di, X. Wang, H. Li, Nano Energy 28 (2016) 447–454.
[40] C. Zhao, X. Zhang, X. Cheng, R. Zhang, R. Xu, P. Chen, H. Peng, Huang Ji, Q. Zhang, Proc. Natl. Acad. Sci. 14 (2017) 11069–11074.
[41] Z. Wan, D. Lei, W. Yang, C. Liu, K. Shi, X. Hao, L. Shen, W. Lv, B. Li, Q.H. Yang, F. Kang, Y.B. He, Adv. Funct. Mater. 4 (2018) 1805301.
[42] H. Duan, Y. Yin, Y. Shi, P. Wang, X. Zhang, C. Yang, J. Shi, R. Wen, Y. Guo, L. Wan, J. Am. Chem. Soc. 140 (2018) 82–85.
[43] D. Chen, Z. Lou, K. Jiang, G. Shen, Adv. Funct. Mater. 28 (2018) 1805596.
[44] P. Han, G. Xu, X. Han, J. Zhao, X. Zhou, G. Cui, Adv. Energy Mater. 8 (2018) 1801243.
[45] J. Sun, X. Zhao, W.R.K. Illeperuma, O. Chaudhuri, K.H. Oh, D.J. Mooney, J.J. Vlassak, Z. Suo, Nature 489 (2012) 133–136.
[46] Y. Xiao, L. Jiang, Z. Liu, Y. Yuan, P. Yan, C. Zhou, J. Lei, Polym. Test. 60 (2017) 160–165.
[47] D.R. Figueroa, A.V. Chadwick, J.H. Strange, J. Phys. C: Solid State Phys. 11 (1978) 55–73.
[48] C. León, M. Lucía, J. Santamaría, M. París, J. Sanz, A. Varez, Phy. Rev. B 54 (1996) 184–189.
[49] C.E. Tambelli, J.P. Donoso, A.M. Regiani, A. Pawlicka, A. Gandini, J.F. LeNest, Electrochim. Acta 46 (2001) 1665–1672.
[50] D.F. Ratner, A. Mark, Shriver, Chem. Rev. 109–124 (1988).
[51] W. Young, W. Kuan, T.H. Epps, Polym. Phys. 52 (2014) 1–16.
[52] A. Christie, S. Lilley, E. Staunton, Y. Andreev, P. Bruce, Nature 433 (2005) 50–53.
[53] S. Chen, F. Feng, Y. Yin, X. Liao, Z. Ma, Energy Storage Mater. 22 (2019) 57–65.